FLORE
Repository istituzionale dell'Università degli Studi di Firenze

Pseudo-dynamic tests on two buildings retrofitted with damped braces

(Article begins on next page)
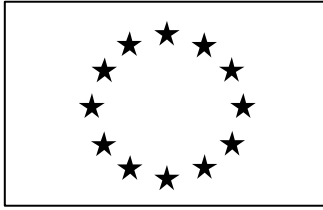
20 July 2024

Pseudo-Dynamic Tests on two Buildings Retrofitted with Damped Braces

J. Molina, G. Magonette, B. Viaccoz, S. Sorace[1], G. Terenzi[2]

[1]Department of Civil Engineering, University of Udine,
Via delle Scienze 208, 33100 Udine, Italy.
[2]Department of Civil Engineering, University of Florence,
Via di S. Marta 3, 50139 Florence, Italy.

LEGAL NOTICE

Neither the European Commission nor any person
acting on behalf of the Commission is responsible for the
use which might be made of the following information.

A great deal of additional information on the
European Union is available on the Internet.
It can be accessed through the Europa server
(http://europa.eu.int)

ABSTRACT

Seismic tests have been conducted on two 3-storey buildings protected with fluid-viscous spring damper devices. One of the buildings was a reinforced concrete frame with clay elements in the slabs, while the other one was a steel frame with steel/concrete composite slabs. The spring dampers were installed through K bracing in between the floors. The tests were performed by means of the pseudodynamic method on full-size specimens and by implementing a specific compensation strategy for the strain-rate effects at the devices. The tests results allowed to compare the behaviour of the unprotected buildings with several protected configurations showing the benefits of the application of the devices and the characteristics of their behaviour.

1 INTRODUCTION

Fluid-viscous damper devices may successfully be used for seismic protection of structures either for energy dissipation or for base isolation (Sorace and Terenzi, 2001ab). These devices operate on the principle of the flow of special compressible fluids through orifices and are characterised by a high cycle-fatigue life and compact size. In order to assess the performance of structures protected with such devices and develop the appropriate numerical models and design method, full-size seismic tests are required that include the attachment system onto the structure.

Seismic testing of large-size models is nowadays possible thanks to the pseudodynamic (PsD) method in large reaction-wall facilities such as the JRC ELSA laboratory of the European Commission (Donea et al., 1996). The alternative of using very large shaking tables when available, for heavy and tall specimens, has serious limitations of accuracy in the application of the input and reproduction of the characteristics of the structure. This is mainly due to the interaction between the specimen and the shaking table.

On the other hand, the PsD method, being a quasistatic technique, may be inadequate for materials showing a strain-rate effect (SRE) in their behaviour unless appropriate compensating techniques are adopted as the ones explained herein. These compensating techniques, when applicable, require a preliminary characterisation of the SRE on the specific material (or device in this case).

2 CHARACTERISING TEST

In order to characterise the cyclic behaviour of one type of dissipater (Jarret BC1BN) to be installed on the specimens, sinusoidal cycles of different decreasing amplitudes (10, 8, 6, 4, 2, 1 and 0.5 mm) were imposed to a single device prestressed at 11 mm, which is the centre of its run. The first amplitude (10 mm) was repeated four times in order to obtain a stabilised behaviour before starting the decreasing amplitude series. Those cycles were applied at a frequency of 2.0 Hz (for the original reference speed) and followed by a random history with significant frequency content up to 6 Hz (Fig. 1). This history of displacement was executed at the nominal reference speed ($\lambda=1$) and then at speeds $\lambda=3$, 10, 30, 100 and 300 times slower in order to analyse the SRE on the measured force.
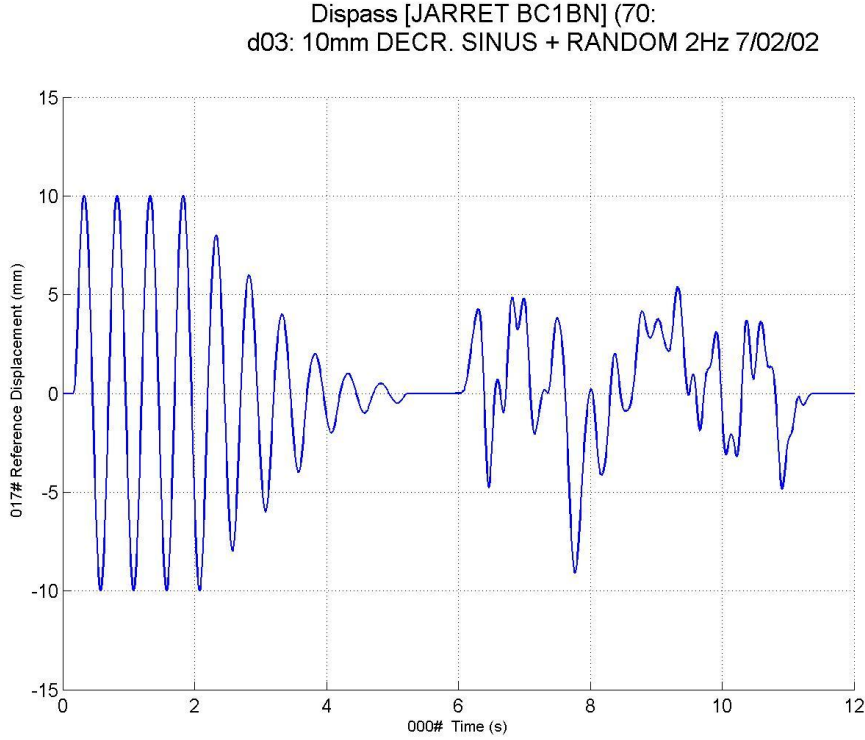
Figure 1. Reference displacement used for the characterising test

2.1 Correction of the strain rate effect

In Figs. 2 and 3, the first two curves respectively represent the measured forces and displacements for the fastest (reference) test at 2 Hz (λ=1) and for the slowest test at 2/300 Hz (λ=300). The displayed time-axis values are the ones at the reference speed. Only the decreasing-sinus part of the test is shown in these two graphs. Due to the strain-rate-effect, the force measured at the slow test has smaller amplitudes, even though the shape is similar to the one at the fast test. This fact suggests a way to correct the force measured at the slow test by multiplying it by a constant factor, which should depend on the testing speed (De Luca et al., 2001, Molina et al., 2000, 2002b). Thus, the corrected force $f_{\lambda=300}^{corr}$ (third curve in the graphs) was obtained as the measured force at the slow test $f_{\lambda=300}^{meas}$ multiplied by constant B plus a constant offset A_o and it should approximate the force at the real speed test $f_{\lambda=1}^{meas}$, that is to say,

$$f_{\lambda=300}^{corr} = B \, f_{\lambda=300}^{meas} + A_o \approx f_{\lambda=1}^{meas} \tag{1}$$

Using the measured forces for the fast and the slow tests during the decreasing sinus, the value of those constants was estimated by least squares as

$$B = 1.184 \qquad\qquad A_o = -0.48 \, \text{kN} \tag{2}$$

Dispass [JARRET BC1BN] (70:
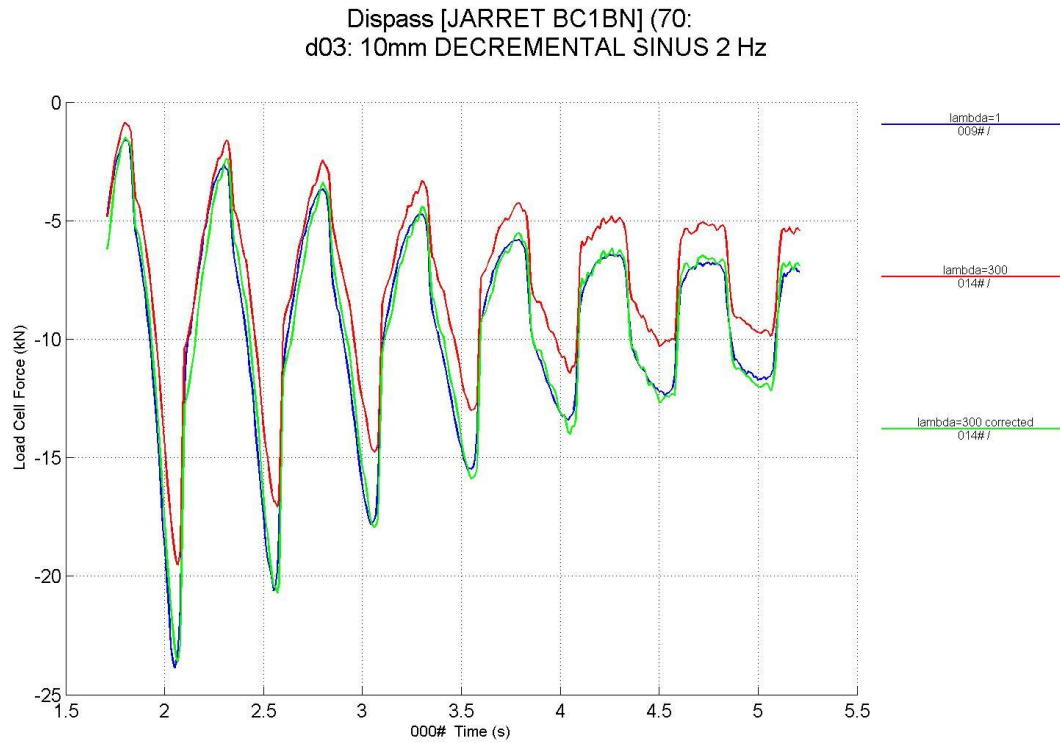d03: 10mm DECREMENTAL SINUS 2 Hz

Figure 2. Force history at reference speed (blue), 300 times slower (red) and 300 times slower after correction (green line). Sinus displacement.

Considering these values, the corrected force was plotted in Figs. 2, 3 as the third curve. One can see how this corrected force significantly reduces the error due to the SRE. Then, applying the same constants to a piece of the random part of the tests (Fig. 4), the effect of the correction can also be assessed for an arbitrary displacement history.

For the case of using two devices acting together with opposite direction, as in the current assemblage specially designed for the two specimens, the offset term A_o would not be needed because the offset of one device would cancel with the one of the other and the corrected force would be obtained just by multiplying by the B factor. Fig. 5 shows the value of the correction factor B obtained for the different tested speeds by using the same method as for the shown case (λ=300). Thus, depending on the speed of the test, the measured forces should be corrected by applying the factor read at this graph.

Dispass [JARRET BC1BN] (70:
d03: 10mm DECREMENTAL SINUS 2 Hz

Figure 3. Force-displacement cycles at reference speed (blue), 300 times slower (red) and 300 times slower after correction (green line). Sinus displacement.

Dispass [JARRET BC1BN] (70:
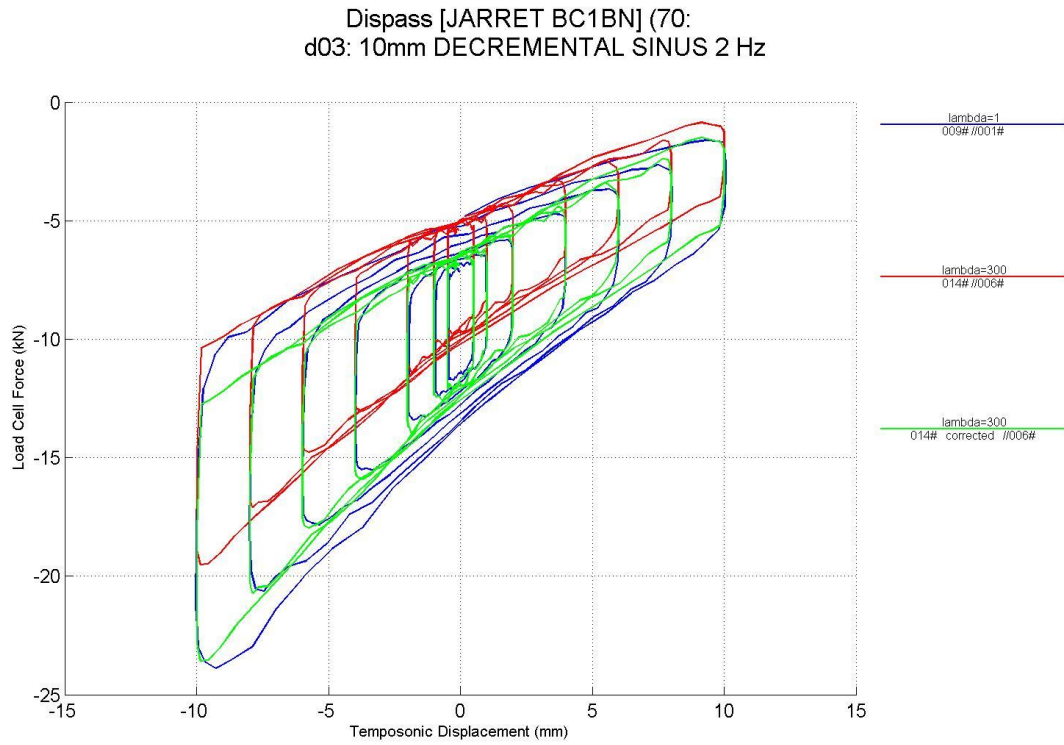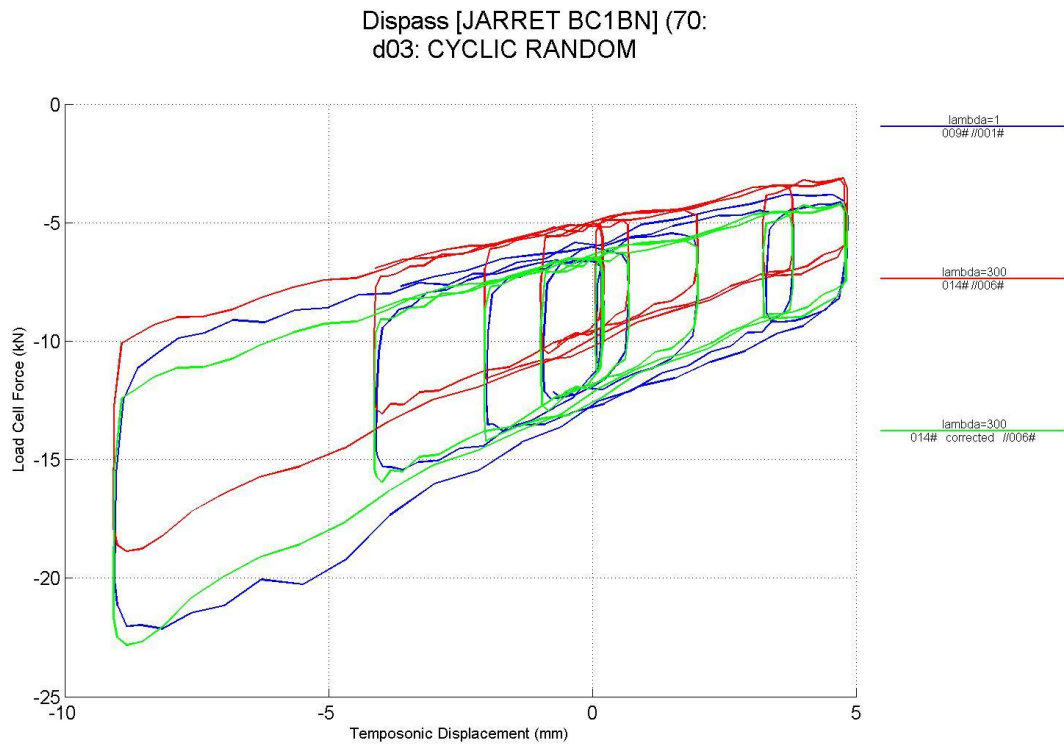d03: CYCLIC RANDOM

Figure 4. Force-displacement cycles at reference speed (blue), 300 times slower (red) and 300 times slower after correction (green line). Random displacement.
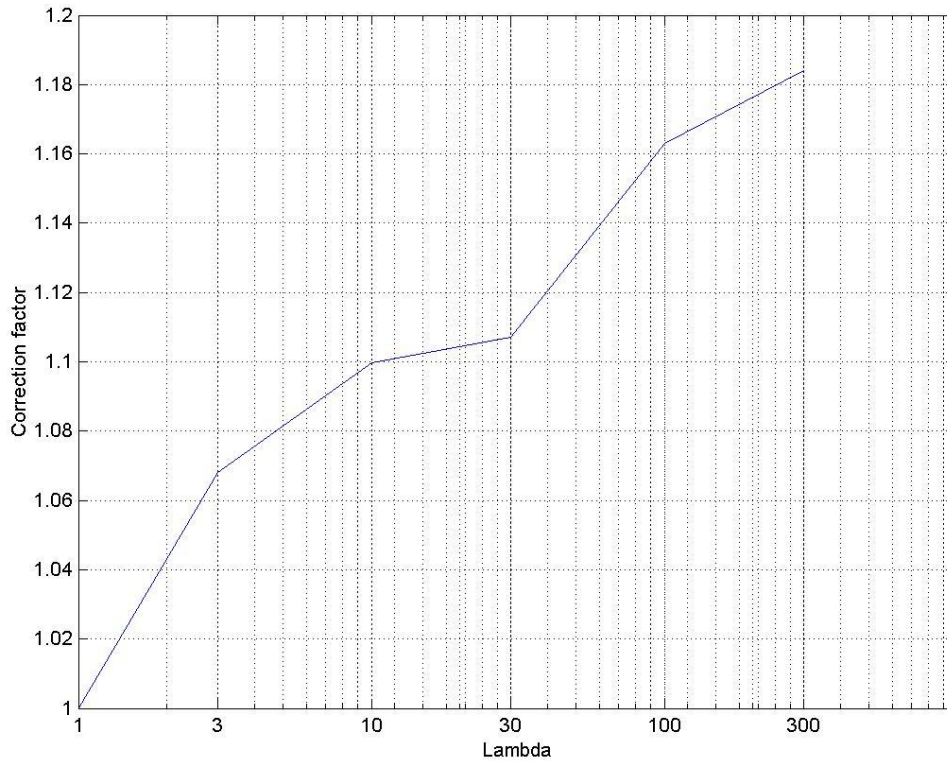
Figure 5. Value of the force-correction coefficient as a function of the testing time scale.

3 TESTING METHOD

3.1 Pseudodynamic Method

The discrete equation of motion

$$\mathbf{Ma} + \mathbf{Cv} + \mathbf{r(d)} = \mathbf{p}(t) \tag{3}$$

is the one assumed within the PsD testing technique. There, $\mathbf{M}$ is the mass matrix, $\mathbf{C}$ is the viscous damping matrix, $\mathbf{a}$, $\mathbf{v}$, $\mathbf{d}$ and $\mathbf{p}$ are respectively the vectors of acceleration, velocity, displacement and external load, which are functions of time t, and $\mathbf{r}$ is the vector of restoring forces, which is a non-linear function of the displacements. Within this model, the entities $\mathbf{M}$, $\mathbf{C}$ and $\mathbf{p}(t)$ are considered as known data, while the forces $\mathbf{r(d)}$ are directly measured on line during the test. Most of the times, an explicit integration scheme is used by which, at every integration step, the computed displacement is quasistatically imposed by hydraulic jacks to the specimen and the required forces are simultaneously measured by load cells. For testing large-size specimens, in many cases this method can be applied with clear advantages with respect to the shaking table technique (Donea et al., 1996, Molina et al., 1999).

3.2 Accelerated continuous PsD testing

A distinction will be made here between the 'classic' and the 'accelerated continuous' method. In the first case of a classic PsD test, every integration time step may take typically at least one second of time in the clock at the laboratory. This allows to impose the ramp of incremental displacements, wait for the stabilisation of the system -before the forces are measured- and compute the next displacement. On the other hand, in the case of an accelerated continuous PsD test, as currently implemented at the ELSA laboratory (Magonette et al., 1998), every integration time step takes just 2 ms. This duration coincides with the sampling period of the controllers of the actuators. Within that short lapse of real time, the computer which is in charge for the control closed-loop algorithm additionally reads the force, integrates one step in the equation of motion and updates the target according to the new computed displacement. Then, the accelerogram history is subdivided in very small time increments (20 μs, for example in the prototype time) so that the corresponding displacement increments can be appropriately followed by the pistons in just 2 ms of real time. Typically, a test time scale of $\lambda = 2$ ms / 20 μs = 100 can be reached for a large size specimen, which could mean being around one order of magnitude faster and still rendering much more accurate results than with a classic PsD test.

3.3 Compensation of the strain-rate effect

Fluid-viscous devices as the ones used in this test may show significant SRE. There, the advantage of the continuous PsD technique is double. On the one hand, the test is faster, which reduces the SRE. On the other hand, the ramp and hold phases at every step become diffused in a continuous movement that avoids the stress relaxation within each step. In fact, the relaxation effect within every step of a classic PsD test results on a force evolution with the shape of saw teeth opening the difficult matter of the selection of the appropriate stabilisation time before measuring the force.

Nevertheless, the speed of the testing equipment is limited by the required accuracy. Thus, the duration of the test is usually from 10 to 300 times longer than the original duration of the event. Fortunately, the considerable SRE still existing at that testing speed may be neutralised by using the compensating strategy proposed herein. Say, for example, that the current testing speed is $\lambda=300$, then, according with Fig. 5, the corresponding correction factor for the forces at the device level is 1.184. Now, instead of using in the integration algorithm the restoring forces measured at the pistons, they are modified by a correction term that is built from the local measure of the force at every dissipator device, multiplied by 1.184-1.0 = 0.184. These correction terms are assembled into a force vector for the structure that is added to the measured restoring forces before it is introduced into the equation of motion.

4   TESTS ON THE FLATSLAB REINFORCED CONCRETE BUILDING

The FLATSLAB building (Negro and Mola, 2002) was designed according to the 1986 Italian Seismic Code for a medium seismicity area. It consists of two RC frames with three storeys and two bays of 6 and 4 metres (Fig. 6). The slabs, with a thickness of 240 mm, are made of 1 m width beams and clay elements with voids. The columns sections are of 400 by 400 mm and the design was made for 0.25 g peak ground acceleration. The protective system, based on damped braces, was designed according to the energy-based

criterion proposed in Sorace and Terenzi 1999, and applied to a retrofit case study in Chiarugi et al. 2000.

Here, the results to four different tests in the longitudinal direction will be commented. The first one was performed on the original specimen without retrofitting with the design accelerogram scaled to 100% while the following three tests were performed on the structure protected with the spring-dampers and for the design accelerogram respectively scaled to 100, 120 and 80%. In the latter cases, the fluid-viscous devices were mounted only at the first two levels by means of steel braces and using a couple of Jarret BC1FN devices for each level of each frame. For every couple, one device was mounted in opposite direction to the other and both of them were prestressed up to the middle of their run that allowed for inter-storey drifts of ±30 mm.
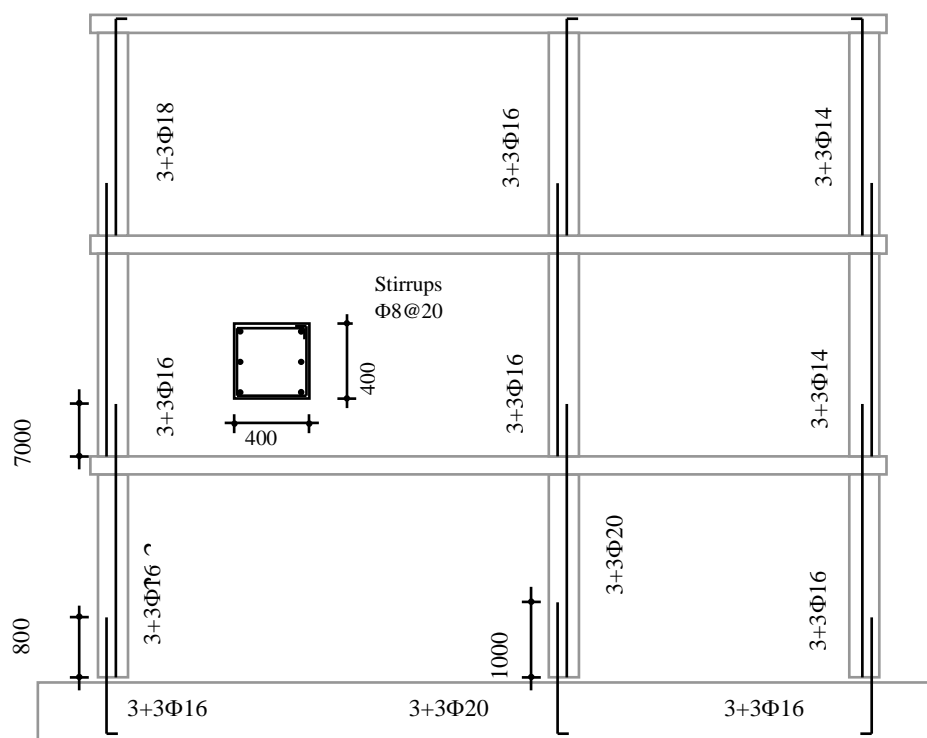
Figure 6. Elevation of the FLATSLAB structure.

Some of the results of those tests are shown in Fig. 7 in terms of consecutive time histories for each one of the tests, that is to say, original structure at 100% of the earthquake with a red curve and retrofitted structure at 100, 120 and 80% of the earthquake with a blue, green and magenta curve, respectively. There, the upper graph shows the displacement at the third level and the middle and lower graphs show the frequency and damping ratio of the first mode. Those modal parameters were estimated by means of an identification method based on a linear–equivalent model. The identification is applied successively to short time windows of the response in order to obtain the evolution of those parameters during the earthquake. At the ELSA laboratory, this technique is usually applied to the results of the seismic tests in order to help in the analysis of the response (Molina et al., 2002a)

Looking at these results, it is clear that with an only value of the eigen frequency and damping ratio it would not be possible to explain the response of this structure to the applied accelerograms. Nevertheless, it is still possible to find a correlation between eigen frequency and oscillation amplitude. To do so, displacement amplitude has been computed by using the Hilbert Transform as obtained through the Fast Fourier Transform (Herlufsen, 1984). This technique has the advantage of being easy to automate. The obtained amplitude has then been averaged over the same time window as the one used for the identification of frequency and damping. The result is shown at the upper graph of Fig.7 in dashed lines.

Now in Fig. 8, for every earthquake, the evolution of the response (solid lines) is traced in an eigen frequency-displacement amplitude axis system. At the same time, in the same axis, the linear response spectrum is represented for every earthquake (dashed lines) for a damping ratio indicated in that figure and corresponding more or less to the identified damping ratio in Fig.7 at the moment in which the displacement was maximum. For consistency, those spectra were also computed based on averaged displacement amplitude and were particularised for the third floor of a linear-shape first mode.

Looking at the correlation between frequency and displacement amplitude (Fig. 8), one can clearly distinguish the earthquake on the original structure from the ones on the retrofitted building. In the first case, the unprotected structure was still completely undamaged at the beginning of the earthquake and the frequency decays are associated to increased levels of damage due to the maximum attained displacement at every moment. That is the reason way, when the amplitude decays from about 64 to 20 mm, the frequency remains almost unchanged at around 1.05 Hz (in Fig. 7 this happens at around 11 s of the earthquake).

In the case of the earthquakes applied to the structure protected with the spring-dampers, there was not additional damage during the earthquake and the variation in frequency is just due to the variation of the displacement amplitude. At the device level (Figs. 3, 4), for very small amplitude displacements, the stiffness can be very high but then, when the flow in the devices starts for larger displacements, the stiffness decreases very rapidly up to a minimum which is determined by the compressibility of the fluid. This is translated into a strong change in the frequency of the first mode when the displacement grows up to 20 mm but afterwards the frequency remains almost constant at 1.2 Hz (Fig. 8).

Another interesting observation from the same Fig. 8 is that the intersection of that displacement-frequency curve with the corresponding response spectrum for every earthquake is roughly verified at the maximum displacement amplitude obtained during the test. That fact should be exactly verified for an invariant linear one-DoF structure.
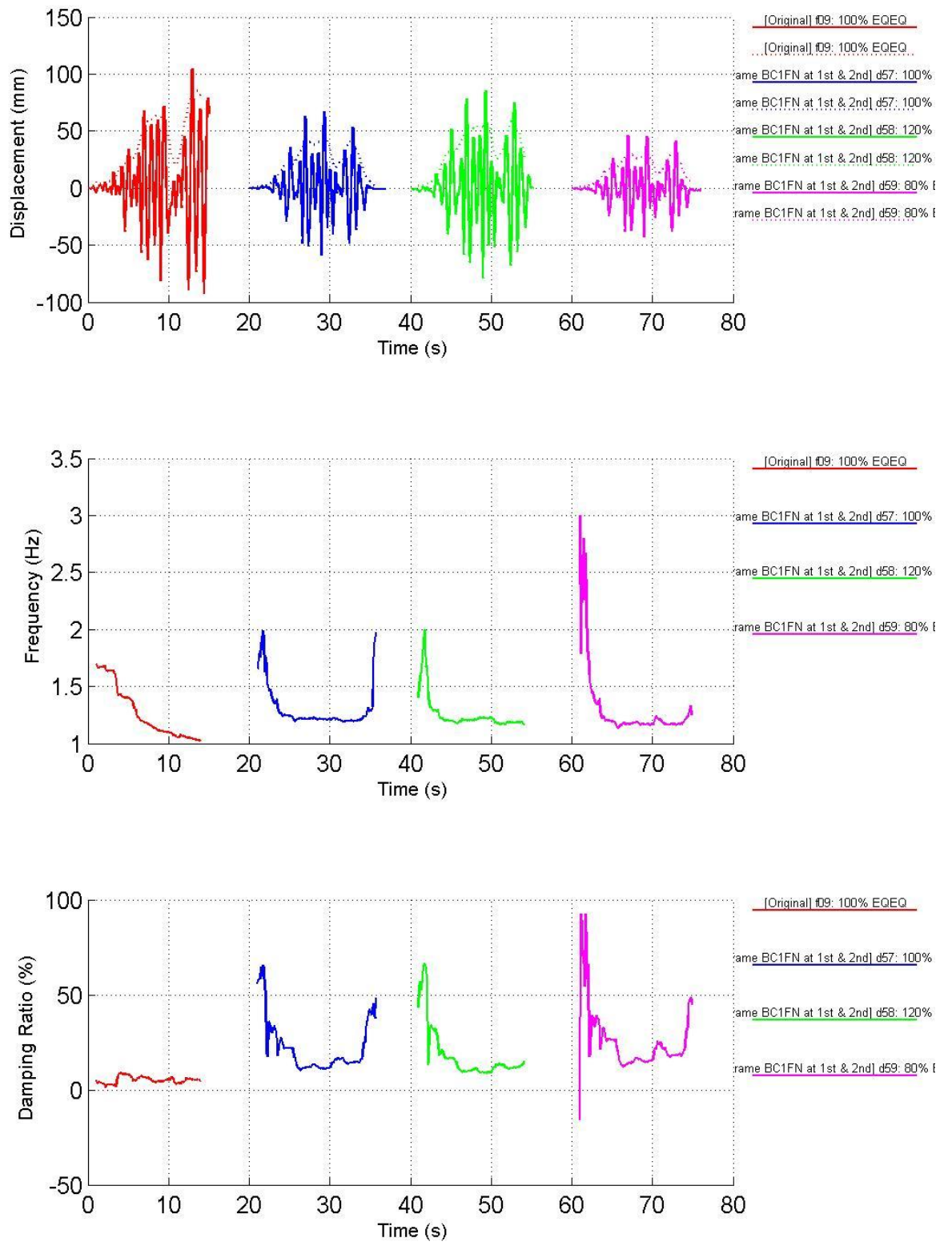
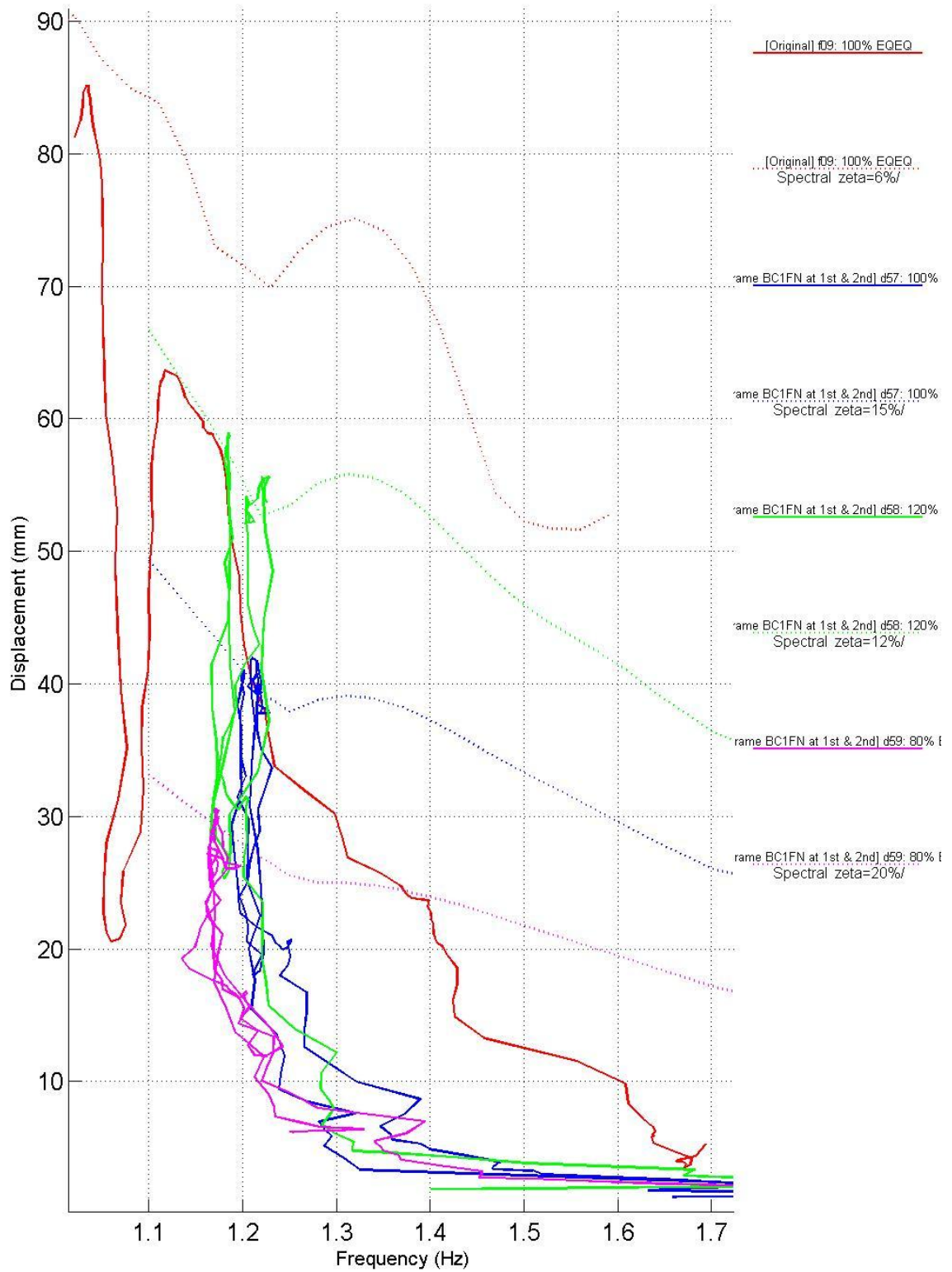Figure 7. FLATSLAB structure. Time-history response.

Figure 8. FLATSLAB structure. Displacement-frequency correlation.

In a similar way, in Fig. 9, every curve represents the evolution of the displacement amplitude as a function of the damping ratio for each one of the earthquakes. Again the behaviour during the earthquake on the original unprotected structure is clearly distinct from the ones on the retrofitted building. In the first case the damping oscillates between 3 and 9% and has only a slight tendency to grow with the displacement (mainly at the moment in which the damage is produced). On the other hand, for the structure protected with the devices, the behaviour is very repetitive and the damping ratio shows a strong tendency to decrease when the displacement increases. This behaviour is typical of systems with constant damping (or friction) force and constant stiffness because there, for every cycle, the dissipated energy is proportional to the displacement amplitude while the elastic energy is proportional to the square of the displacement amplitude. Thus, since the equivalent damping ratio is proportional to the quotient of both energies, it turns to be inversely proportional to the displacement amplitude. This behaviour is not common in conventional structures that show increased damping characteristics for increased displacements as a consequence of the correspondingly increased levels of induced damage.

5   TESTS ON THE BABYFRAME STEEL-CONCRETE COMPOSITE BUILDING

The BABYFRAME building consists of a steel frame with three reinforced concrete floors (see Fig. 10). The frame has two longitudinal bays by one transversal bay. The size of the longitudinal bays is 4 m each while that of the transversal bay is 2.5 m. The height of the floors is 2 m each. The profiles of the columns are HEB140 and those of the longitudinal and transversal beams are IPE180 being made all of them of standard steel Fe360. Beam-to-column connections are welded and stiffened. The reinforced concrete slabs were poured on corrugated steel sheet that was clamped to the beams by nails. The specified earthquake for this structure was of 30% g. As for the previous example, the protective system was designed according to the energy-based criterion proposed in Sorace and Terenzi 1999.

Here the results to four different tests in the longitudinal direction will be commented. The first one was performed on the original specimen without retrofitting and for the specified accelerogram scaled to 100%. The second one refers to the structure protected with Jarret BC1BN devices (±11 mm) at every level and for 100% of the accelerogram. Finally, the third and the fourth tests refer to the structure protected with Jarret BC1BN devices at the first and third levels, plus BC1DN devices (±17.5 mm) at the second level and for 100 and 150% of the accelerogram respectively. As in the case of the FLATSLAB structure, the spring-dampers were mounted by means of steel braces and using a couple of prestressed devices for each level of each frame. In the second protected configuration, larger devices (BC1DN) were used at the second level in order to allow for larger drifts and forces at this position, which corresponds with the shape of the first mode of the structure.
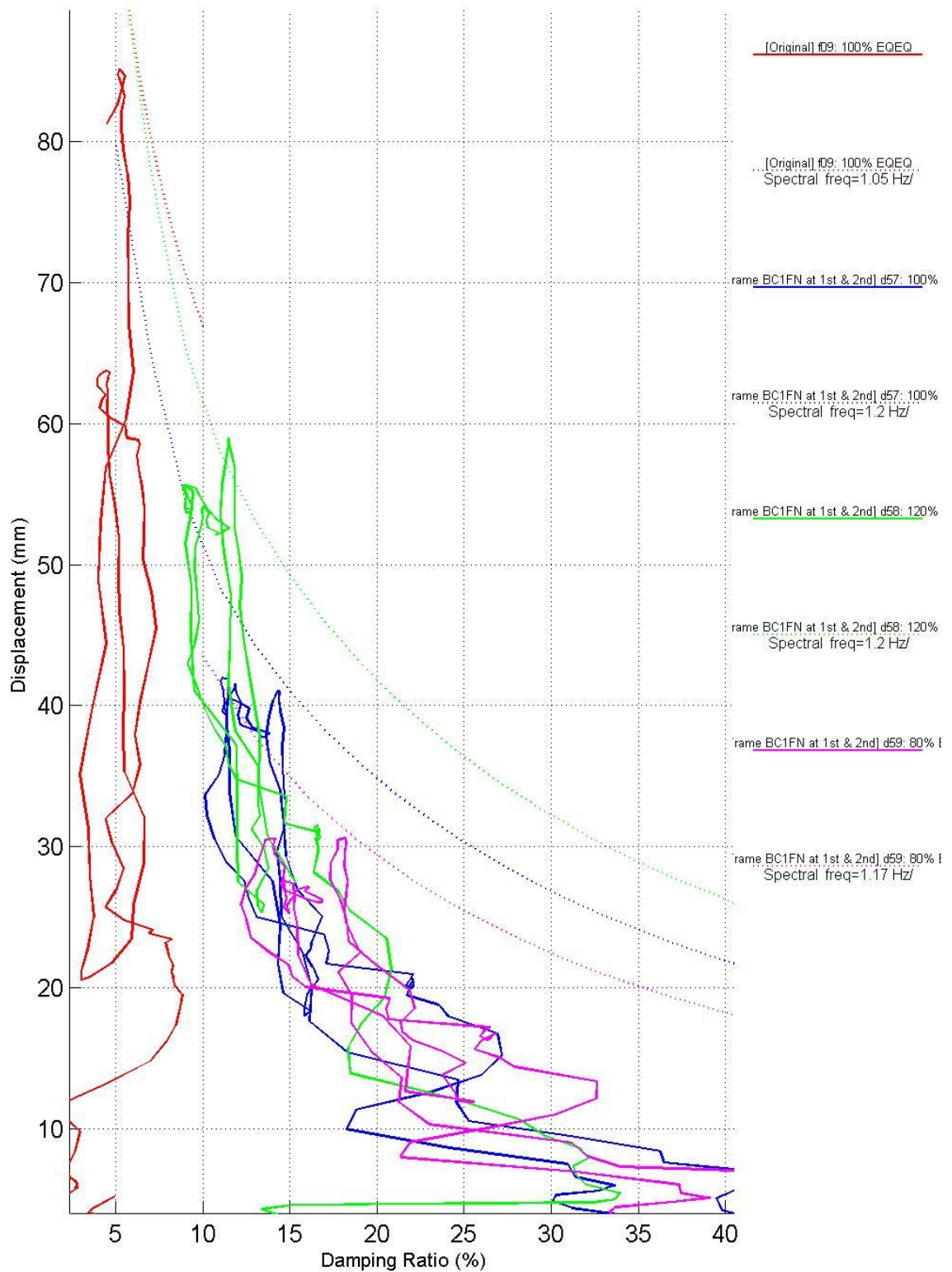
Figure 9. FLATSLAB structure. Displacement-damping correlation.

In a similar way as for the previous structure, some of the results of the tests are shown in Fig. 11 in terms of consecutive time histories for each one of the tests, that is to say,

original structure at 100% of the earthquake with a red curve, structure protected with BC1BN devices at every level and for 100% of the accelerogram with a blue curve and, then, the structure protected with BC1BN devices at the first and third levels, plus BC1DN devices at the second level and for 100 and 150% of the accelerogram with a green and a magenta curve, respectively. Also similarly to the previous example, Figs. 12 and 13 show the correlations of the displacement amplitude at the third level with, respectively, the frequency and the damping ratio of the first mode.
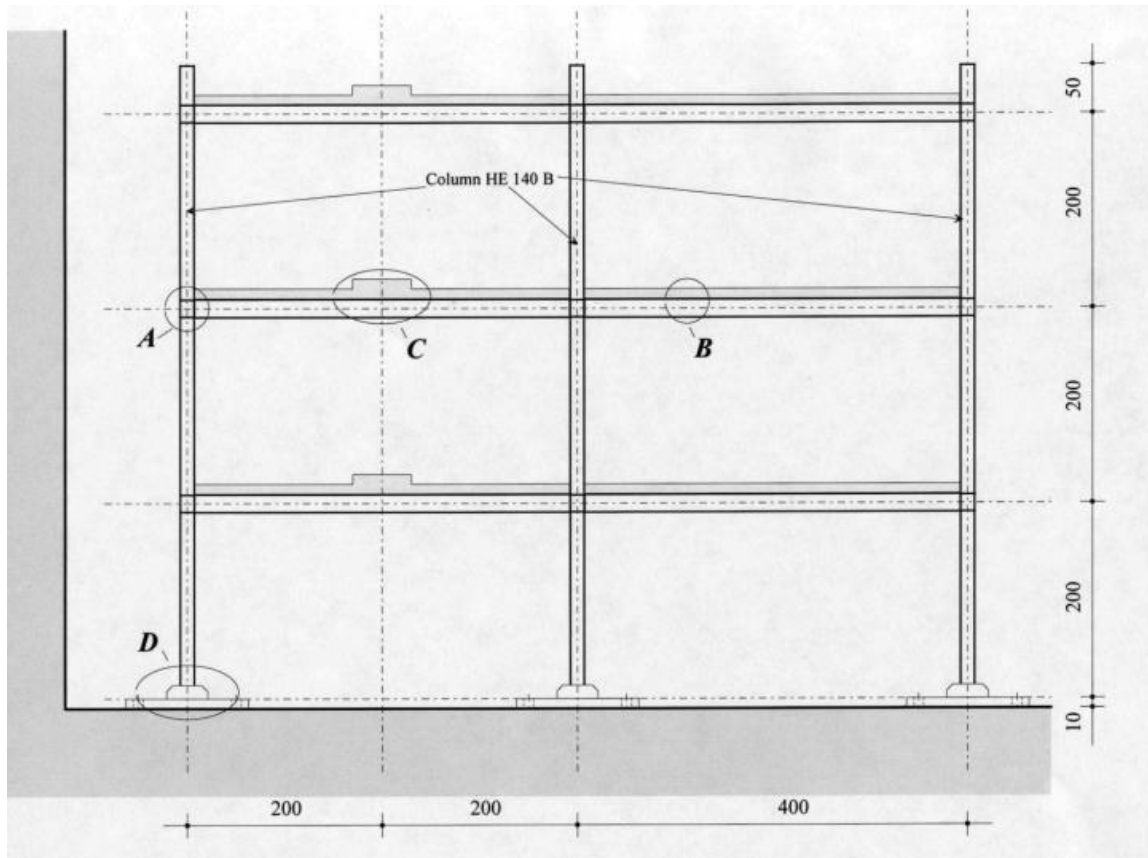

Figure 10. Elevation of the BABYFRAME structure.

Again, either in Fig. 12 or 13, a clear difference in the behaviour is observed for the original structure with respect to the protected cases. Moreover, the green and the magenta curves refer to a protected configuration that is different to the one of the blue curve and this is also slightly reflected in the behaviour. In general, the introduction of the devices increases the frequency and the damping ratio and in the case with larger devices at the second level (green and magenta curves) these effects are larger.

Looking more in detail at the displacement-frequency correlations in Fig. 12, one can observe that, contrarily to the FLATSLAB example, the frequency is rather constant during each test. In the first configuration (unprotected frame) this is logic because the deformations were absorbed by the steel frame without introducing appreciable damage. On the other hand, in the protected configurations, the presence of the devices did not result in a variable frequency during the tests because the observed deformations were always relatively large in comparison with the run of the adopted devices. The inverse proportionality between damping ratio and displacement amplitude is also observed for this structure when retrofitted with the spring-damper devices (Fig. 13).
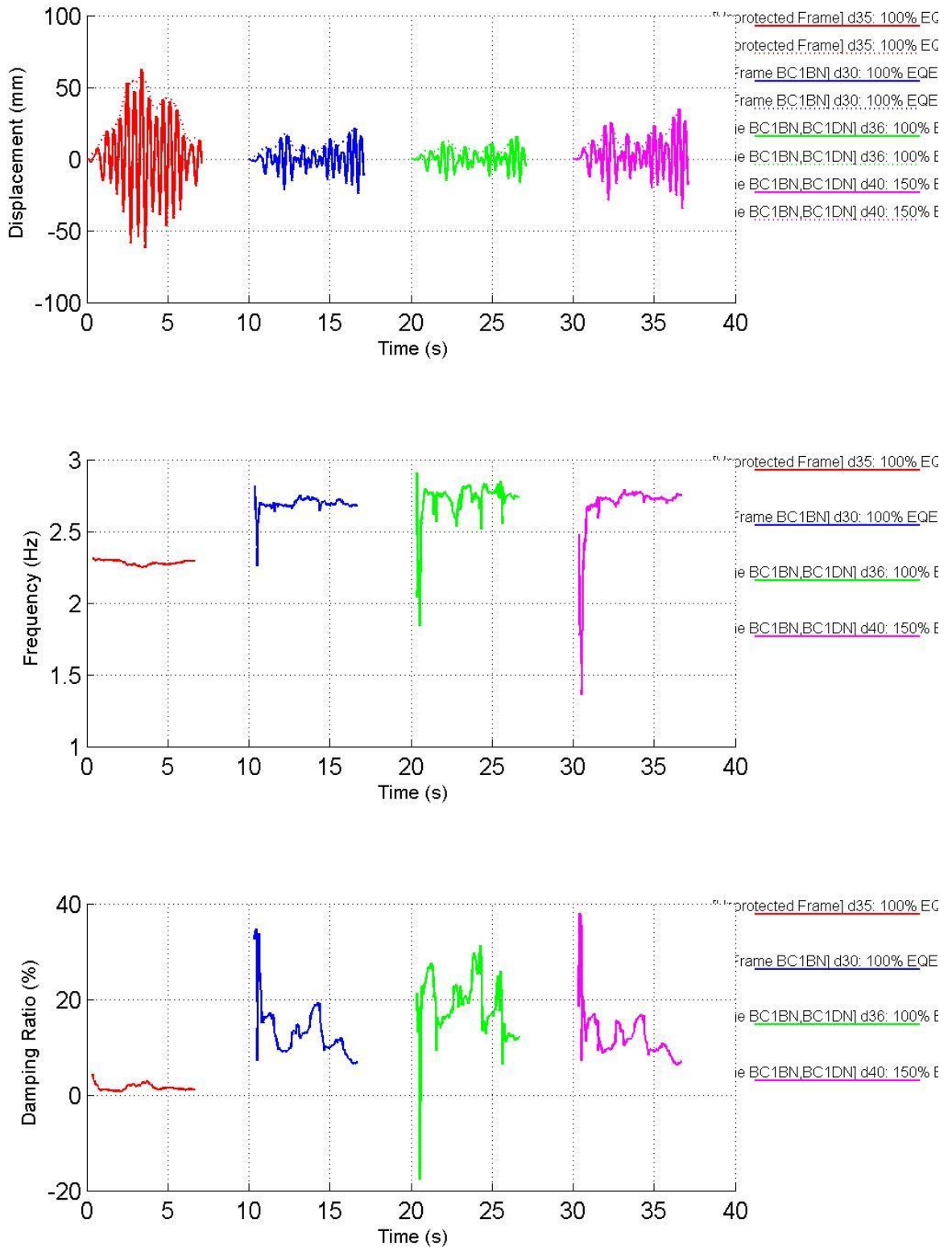
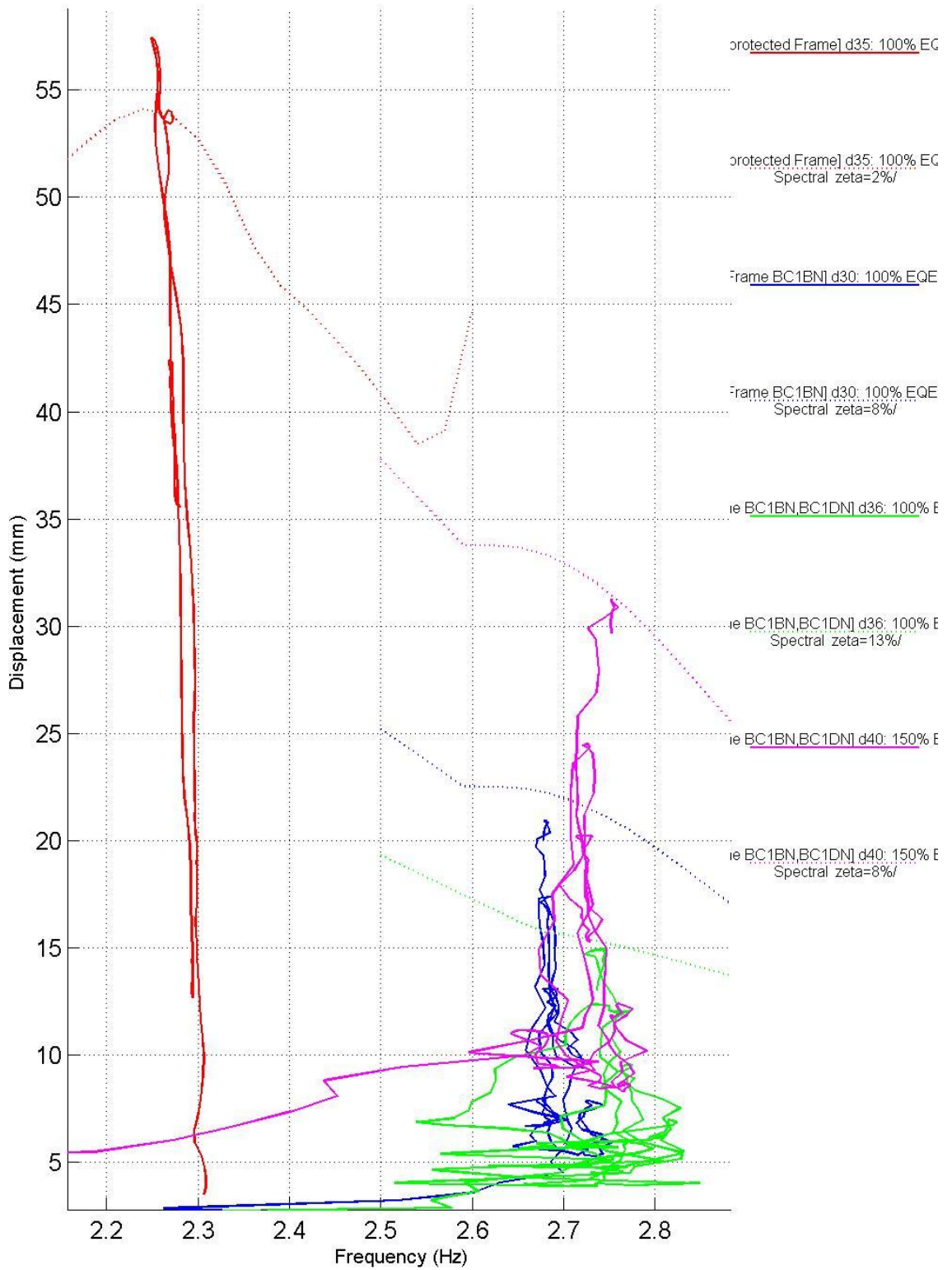Figure 11. BABYFRAME structure. Time-history response.

Figure 12. BABYFRAME structure. Displacement-frequency correlation.
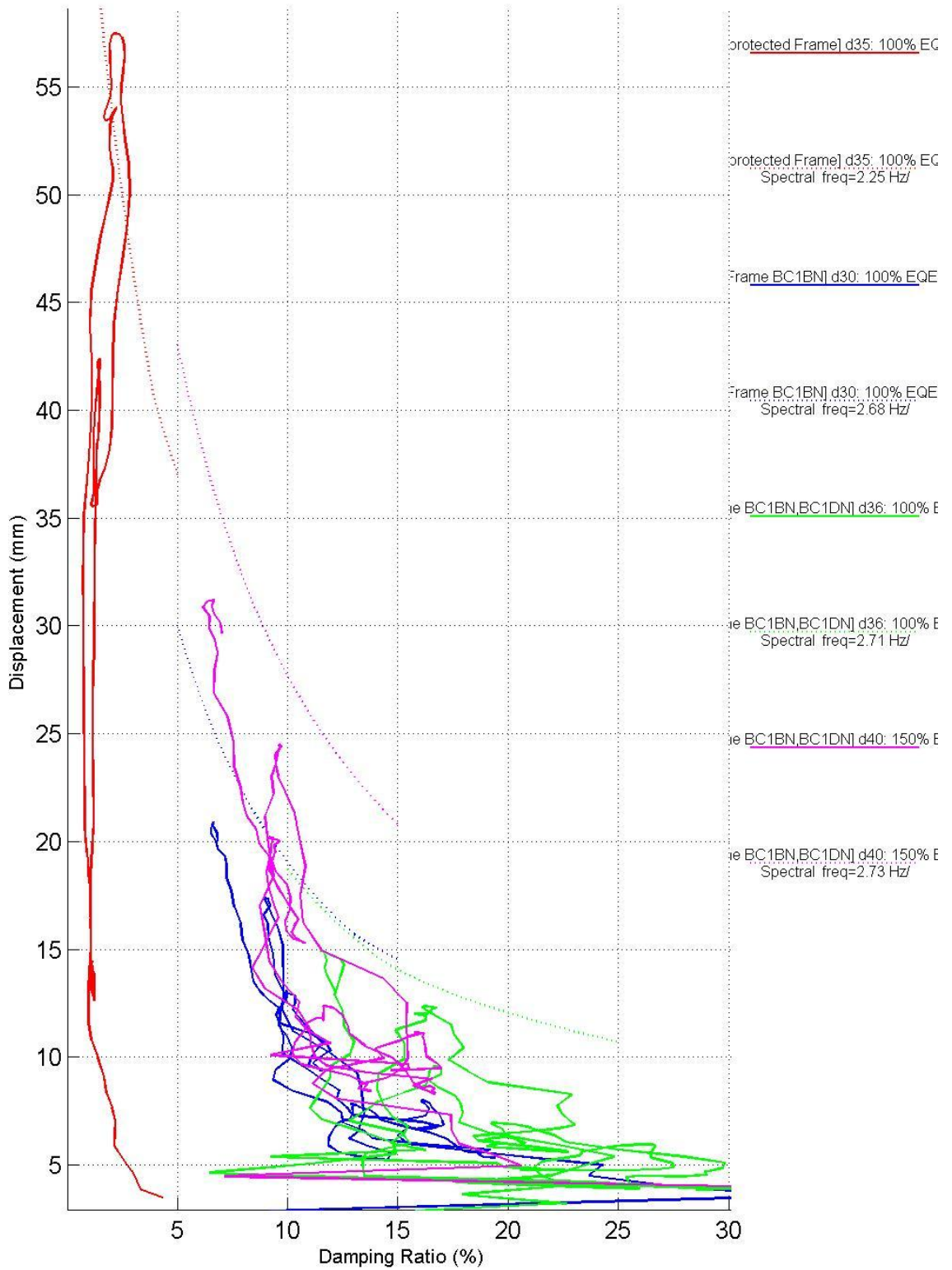
Figure 13. BABYFRAME structure. Displacement-damping correlation.

6   CONCLUSIONS

Fluid-viscous spring-damper devices may show significant SRE that may render inadequate a PsD test performed on structures protected with such kind of devices. However, by combining the continuous PsD method with the proposed restoring-force correction technique, those SRE errors can be drastically minimised as here shown.

Fluid-viscous devices installed through braces may protect a structure by means of altering its stiffness and, more effectively, its damping characteristics as it was shown in the examples. Even though in some cases the applied earthquake was more intense than the reference one, the response was always smaller in the retrofitted models.

For the RC FLATSLAB structure, the first reference earthquake on the unprotected building introduced some damage (which changed its frequency) while the earthquakes imposed to the protected structure did not cause any additional damage as observed from the response displacement-frequency and displacement-damping correlations.

For the case of the steel concrete composite BABYFRAME structure, none of the earthquakes caused significant damage, but the retrofitting reduced the response also in this case.

7   REFERENCES

1. Chiarugi, A., Sorace, S., and Terenzi, G. (2000), Effectiveness of viscous damped bracing systems for steel frames, *Proceedings of the Third International Conference on the Behaviour of Steel Structures in Seismic Areas, STESSA 2000*, Montreal, 379-385.
2. De Luca, A., Mele, E., Molina, F. J., Verzeletti, G. and Pinto, A. V. (2001), Base isolation for retrofitting historic buildings: evaluation of seismic performance through experimental investigation, *Earthquake Engineering & Structural Dynamics*, 30, 1125-1145.
3. Donea, J., Magonette, G., Negro, P., Pegon, P., Pinto, A., and Verzeletti, G. (1996), Pseudodynamic Capabilities of the ELSA Laboratory for Earthquake Testing of Large Structures, *Earthquake Spectra*, 12, 163-180.
4. Herlufsen, H. (1984), *Dual Channel FFT Analysis (Part II)*, Brüel & Kjaer Tech. Rev. No. 2.
5. Magonette, G., Pegon, P., Molina, F. J. and Buchet, Ph. (1998), Development of fast continuous substructuring tests, *Proceedings of the Second World Conference on Structural Control,* Kyoto.
6. Molina, F. J., Verzeletti, G., Magonette, G., Buchet, Ph., and Géradin, M. (1999), Bi-directional pseudodynamic test of a full-size 3-storey building, *Earthquake Engineering & Structural Dynamics*, 28, 1541-1566.
7. Molina, F. J., Verzeletti, G., Magonette, G., and Taucer, F. (2000), Dynamic and Pseudodynamic responses in a two storey building retrofitted with rate-sensitive rubber dissipators, *Proceedings of the 12th World Conference on Earthquake Engineering*, Auckland, paper 634.
8. Molina, J., Magonette, G. and Pegon, P. (2002a), Assessment of systematic experimental errors in pseudodynamic tests, *Proceedings of the 12th European Conference on Earthquake Engineering*, London, paper 525.
9. Molina, J., Verzeletti, G., Magonette, G., Buchet, Ph., Renda, V., Geradin, M, Parducci, P., Mezzi, M., Pacchiarotti, A., Federici, L. and Mascelloni, S. (2002b), Pseudodynamic tests on rubber base isolators with numerical substructuring of the superstructure and strain-rate effect compensation, *Earthquake Engineering & Structural Dynamics*, 31, 1563-1582.

10. Negro, P. and Mola, E. (2002), Current assessment procedures: Application to regular and irregular structures compared to experimental results, *Third European Workshop on the Seismic Behaviour of Irregular and Complex Structures*, EAEE, Florence.
11. Sorace , S. and Terenzi, G. (1999), Iterative procedure for the design of fluid viscous devices included in braced frames, *Proceedings of the 4th European Conference on Structural Dynamics, Eurodyn '99*, Prague, Checz Republic, Vol. 1, pp. 169-174.
12. Sorace, S. and Terenzi, G. (2001a), Non-linear dynamic modelling and design procedure of FV spring dampers for base isolation, *Engineering Structures*, 23, 1556-1567.
13. Sorace, S. and Terenzi, G. (2001b), Non-linear dynamic design procedure of FV spring-dampers for base isolation – Frame building applications, *Engineering Structures*, 23, 1568-1576.
14. Taucer, F. et al. (2002), Equivalent Damping of Fluid Viscous spring-dampers, EC, JRC, Technical Note (in preparation).

Mission of the JRC

The mission of the JRC is to provide customer-driven scientific and technical support for the conception, development, implementation and monitoring of EU policies. As a service of the European Commission, the JRC functions as a reference centre of science and technology for the Union. Close to the policy-making process, it serves the common interest of the Member States, while being independent of special interests, whether private or national.

EUROPEAN COMMISSION
JOINT RESEARCH CENTRE